Journal of Marine Science and Technology

Volume 25 | Issue 6 Article 11

ENERGY EFFICIENT TRAJECTORY DESIGN FOR THE UNDERWATER VEHICLE WITH BOUNDED INPUTS USING THE GLOBAL OPTIMAL SLIDING-MODE CONTROL

Mai The Vu
Department of Convergence Study on the Ocean Science and Technology, School of Ocean and Technology, Korea Maritime and Ocean University, Busan, South Korea.

Hyeung-Sik Choi
Department of Mechanical Engineering, Korea Maritime and Ocean University, Busan, South Korea., hchoi@kmou.ac.kr

Jin-Il Kang
Department of Mechanical Engineering, Korea Maritime and Ocean University, Busan, South Korea.

Dae-Hyung Ji
Department of Mechanical Engineering, Korea Maritime and Ocean University, Busan, South Korea.

Hyun Joong
Department of Mechanical Engineering, Korea Maritime and Ocean University, Busan, South Korea.

Recommended Citation

Vu, Mai The; Choi, Hyeung-Sik; Kang, Jin-Il; Ji, Dae-Hyung; and Joong, Hyun (2017) "ENERGY EFFICIENT TRAJECTORY DESIGN FOR THE UNDERWATER VEHICLE WITH BOUNDED INPUTS USING THE GLOBAL OPTIMAL SLIDING-MODE CONTROL," *Journal of Marine Science and Technology*: Vol. 25: Iss. 6, Article 11.
DOI: 10.6119/JMST-017-1226-11
Available at: https://jmstt.ntou.edu.tw/journal/vol25/iss6/11

ENERGY EFFICIENT TRAJECTORY DESIGN FOR THE UNDERWATER VEHICLE WITH BOUNDED INPUTS USING THE GLOBAL OPTIMAL SLIDING-MODE CONTROL

Acknowledgements

This research is a part of the project National Research Foundation of Korea (NRF-2016R1A2B4011875) and a part of project titled "R & D center for underwater construction robotics", South Korea (PJT200539), funded by the Ministry of Oceans and Fisheries (MOF).

Journal of Marine Science and Technology, Vol. 25, No. 6, pp. 705-714 (2017)
DOI: 10.6119/JMST-017-1226-11

ENERGY EFFICIENT TRAJECTORY DESIGN FOR THE UNDERWATER VEHICLE WITH BOUNDED INPUTS USING THE GLOBAL OPTIMAL SLIDING-MODE CONTROL

Mai The Vu[1], Hyeung-Sik Choi[2], Jin-Il Kang[2], Dae-Hyung Ji[2], and Hyun-Joong[2]

Key words: underwater vehicle (UV), sliding mode control, bounded inputs, time optimal trajectory, uncertainty.

ABSTRACT

In this paper, we propose a novel global sliding mode controller (SMC) for an uncertain linear time-varying second order system. The proposed controller was implemented on the underwater vehicle (UV) with uncertainty of bounded parameters and disturbances within limited control input. By applying the proposed controller to the second-order UV system, the arrival time at the reference position and the maximum allowable acceleration are expressed in a closed-form equation if ranges of parametric uncertainties and reference inputs are specified. The closed-form equation can be utilized in designing the capacity of vehicle systems with the condition of the minimum arrival time to the target position. The superior performance of the proposed control scheme is validated through computer simulation. The simulation results show that this proposed controller forces the UV to track the designed time optimal trajectory very well, even with uncertainties. Its robustness can be guaranteed if bounds of the uncertainties are known.

I. INTRODUCTION

Nowadays, autonomous underwater vehicles (AUVs) have become a main tool for surveying the undersea for scientific, military, and commercial applications. Despite of the considerable improvement in AUV performance, AUV technologies are still an attractive challenging field to scientists and engineers. Multiple AUVs and underwater docking are recent challenging issues in the field of AUV technologies (Fiorelli et al., 2004; Stokey et al., 2001). Deam and Given (1983) summarized the vast research on the ROV, and proposed five steps to develop ROV. Stewart and Auster (1989) submitted a low-cost technology for developing the ROV, which is helpful to designers in related fields. Out of many issues, study on optimal time or optimal energy one is important due to the existing problem of limitation of battery loading in the UV. However, only a number of studies on the topics of time-optimal and energy-efficient maneuvers for the AUVs have been studied. Recently, Chyba et al. (2008a, b) presented a numerical method for designing the time-optimal trajectory (Chyba et al., 2008a) or the weighted consumption and time-optimal trajectory (Chyba et al., 2008b). However, they are the results of a numerical solver which is difficult to use. An analytical solution for this issue is expected, and is a new challenge.

Moreover, studying on motion control of UVs has attracted attention of many researchers in recent years. In particular, depth control is one of the important issues, indispensable to any AUV. The controllers based on PID techniques have advantages such as: simple, easy to design and to apply (Prestero, 2001). However, they have poor robustness in face of uncertainties, particularly in model uncertainty. To meet the requirements to improve the performance of AUVs, especially in robust control area, advanced control theories have been studied such as: LQG/LTR, H_∞ (Moreira and Guedes Soares, 2008); adaptive nonlinear controller to take free pitch motion (Li and Lee, 2005); and diverse approaches towards the sliding mode control (SMC) such as typical SMC (Healey and Lienard, 1993), adaptive SMC using linear vehicle model (Cristi et al., 1990), SMC using simplified nonlinear model (Rodrigues et al., 1996), high order SMC (Salgado-Jimenez et al., 2004), and optimal SMC (Josserand, 2006). The simple controllers designed on the basis of such a model without considering the effect of uncertainties may face the problems of stability and bad performance in actual operation. The global sliding mode method allows designers not only to overcome these issues but also to be able to keep the controller's performance within desired boundaries in face of input and output disturbance (such as an underwater current), sensor noises, etc. Furthermore, for

Paper submitted 09/14/17; revised 10/18/17; accepted 10/30/17. Author for correspondence: Hyeung-Sik Choi (e-mail: hchoi@kmou.ac.kr).
[1] Department of Convergence Study on the Ocean Science and Technology, School of Ocean and Technology, Korea Maritime and Ocean University, Busan, South Korea.
[2] Department of Mechanical Engineering, Korea Maritime and Ocean University, Busan, South Korea.

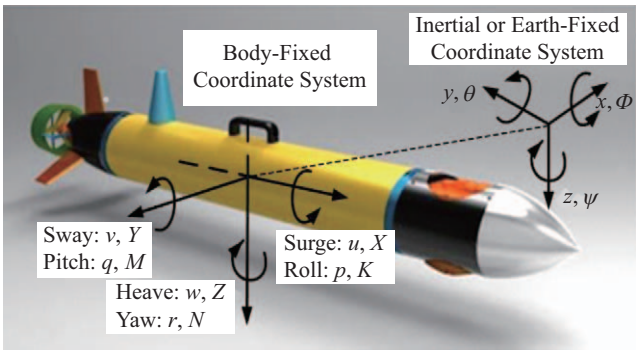

Fig. 1. Body-fixed and inertial coordinate systems.

underwater vehicle robustness, the energy issue is important. By applying proposed SMC, the robustness along with efficient energy trajectories (EETs) of UV would be achieved.

In this paper, new approach is proposed in finding the EETs, together with a robust tracking controller. An analytical method, not a numerical method, is used to find the optimal trajectory for the depth control of the UV. The result of the control action is given in closed-form expressions. The use of such functions increases the controller's automatic ability, and helps to avoid the weaknesses of the numerical method. For the depth controller for the UV, sliding mode control method is applied and its desired trajectory is designed as optimal time or energy efficiency as long as its references (inputs) are the time-optimal or EETs. The simulation results show that this proposed controller forces the UV to track the designed time optimal trajectory very well, even with uncertainties.

II. EQUATIONS OF UV MOTION

1. Assumptions

The dynamic equations of UV are used in the design process of the optimal trajectories and EETs. These dynamic equations are given with the following assumptions:

(1) The vehicle is deeply submerged in a homogeneous, unbounded fluid (the vehicle is located far from free surface-no surface effects).
(2) The effects of the vehicle passing through its own wake are ignored.
(3) The vehicle propeller is a source of constant thrust and its torque is small, thus ignored.
(4) Only the depth motion is considered in this paper.

2. Depth Motion of UV

To derive the dynamic equations for an UV, the two coordinate systems are defined as indicated in Fig. 1. The coordinate *EXYZ* represents the Earth-fixed coordinate system and the coordinate *Bxyz*, which is attached the center of buoyancy of an UV, represents the body-fixed coordinate system. In the body-fixed coordinate system, the positive *x*-direction is the longitudinal axis directed from the stern to the bow, the positive *y*-direction is the transverse axis directed to the starboard, and the positive *z*-direction is the normal axis directed from the top to the bottom. The six Degrees of Freedom (DOF) nonlinear equations of motion for an UV are described in Fossen (1994).

$$
\begin{aligned}
&m\left[\dot{u}-vr+wq-x_G\left(q^2+r^2\right)+y_G\left(pq-\dot{r}\right)+z_G\left(rp+\dot{q}\right)\right]=X\\
&m\left[\dot{v}-wp+ur-y_G\left(r^2+p^2\right)+z_G\left(qr-\dot{p}\right)+x_G\left(pq+\dot{r}\right)\right]=Y\\
&m\left[\dot{w}-uq+vp-z_G\left(p^2+q^2\right)+x_G\left(rp-\dot{q}\right)+y_G\left(qr+\dot{p}\right)\right]=Z\\
&I_{xx}\dot{p}-\left(I_{yy}-I_{zz}\right)qr-I_{yz}\left(q^2-r^2\right)+I_{xy}\left(rp-\dot{q}\right)-I_{zx}\left(pq+\dot{r}\right)\\
&\qquad+m\left[y_G\left(\dot{w}-uq+vp\right)-z_G\left(\dot{v}-wp+ur\right)\right]=K\\
&I_{yy}\dot{q}-\left(I_{zz}-I_{xx}\right)rp-I_{zx}\left(r^2-p^2\right)+I_{yz}\left(pq-\dot{r}\right)-I_{xy}\left(qr+\dot{p}\right)\\
&\qquad+m\left[z_G\left(\dot{u}-vr+wq\right)-x_G\left(\dot{w}-uq+vp\right)\right]=M\\
&I_{zz}\dot{r}-\left(I_{xx}-I_{yy}\right)pq-I_{xy}\left(p^2-q^2\right)+I_{zx}\left(qr-\dot{p}\right)-I_{yz}\left(rp+\dot{q}\right)\\
&\qquad+m\left[x_G\left(\dot{v}-wp+ur\right)-y_G\left(\dot{u}-vr+wq\right)\right]=N
\end{aligned}
\tag{1}
$$

where, m denotes the mass of a vehicle and I_{ij} are the moments of inertia for each axis of subscripts; x_G, y_G, and z_G denote the vehicle's mass center; X, Y, Z, K, M, and N denote the external forces and moments acting on the vehicle represented in the body-fixed coordinate system. These equations that are including the hydrodynamic forces and moments can be expressed in a more compact form as Eqs. (2)-(4).

$$M_v\dot{v}+C_v(v)v+D_v(v)v+G_v(\eta)=\tau_v \tag{2}$$

$$M_v=M_{RB}+M_A \tag{3}$$

$$C_v(v)=C_{RB}(v)+C_A(v) \tag{4}$$

where v is the body-fixed linear and angular velocity vector; M_v is the inertia matrix of the underwater vehicle; C_v is the Coriolis and centripetal terms of the underwater vehicle; D_v is the hydrodynamic lift and damping matrix; G_v represents the restoring forces and moments; τ_v is a generalized vector of external forces and moments.

Full equations of motion of an underwater vehicle can be found as shown in Eq. (1). However, in this paper, we just focus on depth control. So, the nonlinear second order differential equation representing pure depth-plane motion of the vehicle is expressed as:

$$(m-Z_{\dot{w}})\dot{w}-Z_{w|w|}w\,|\,w\,|=(W-B)+T_{zprop} \tag{5}$$

where m, $Z_{\dot{w}}$, w, $Z_{w|w|}$, W, B, T_{zprop} are mass of UV, added mass coefficient, the instantaneous velocity, cross-flow drag coefficient, the weight of UV, the buoyancy force and thrust force, respectively.

Eq. (5) can be rearranged as:

$$(m - Z_{\dot{w}})\ddot{z} - Z_{w|w|}\dot{z} \mid \dot{z} \mid = (W - B) + T_{zprop} \tag{6}$$

where $\dot{z} = w$

By-setting $A = m - Z_{\dot{w}}$, $C = -Z_{w|w|}$, $N = B - W$ and $U = T_{zprop}$, Eq. (6) becomes:

$$A\ddot{z} + C\dot{z} \mid \dot{z} \mid + N = U \tag{7}$$

where A is the combined mass coefficient, $C > 0$ cross-flow drag coefficient, N net buoyancy, U thrust force, and z depth.

III. DESIGN ENERGY EFFICIENT TRAJECTORIES

In Loc et al. (2014), the vehicle is propelled at a high velocity, and comes very close to the destination before entering the deceleration period. This way helps the vehicle move quickly to the destination; however, it obliges the vehicle to use a high reverse force (U_1) to brake the velocity quickly in the deceleration period, in order to stop right at the destination at the end of this period. This method brings the benefit of saving time, but wastes energy. It could not utilize the accumulated kinetic energy, but also spend more energy to eliminate it - a double waste.

In this study, we just discuss EETs applied for driving the vehicle in mode of moving down. Because the vehicle buoyancy is usually made slightly greater than the vehicle weight (the positive net buoyancy, $N = B - W > 0$, allows the vehicle to float to the surface in the event of a failure), in mode of moving up, the best energy-saving control way is to turn off all the thrusters and let the vehicle float slowly to the desired position. For EETs, our control strategy is to use the thrust force at which the efficiency of thruster(s) is maximum, named the highest efficient thrust force U_2 (the corresponding net force F_2), in the constant velocity and acceleration periods; and not to use any reverse thrust force, i.e., the thrust force U_1 is zero (net force F_1), to brake the vehicle velocity in the deceleration period. We will let the vehicle drift to the destination without propulsion in the latter period. We have $F_1 = U_1 - N = -N$, $F_2 = U_2 - N$. With this strategy, the travel time is longer; in return, the energy consumption is minimized.

We will design EETs for the vehicle when it moves from the beginning depth z_0 at time t_0 (z_0, $t_0 = 0$) to the ending depth z_e at time t_e ($z_e > 0$). At both these depth levels, the vehicle is at rest ($\dot{z}(t_0) = v_0 = 0$, $\dot{z}(t_e) = v_e = 0$). Depending on the value z_e, there are two plans for the course of the velocity $\dot{z}$. Plan I: if z_e is large, $\dot{z}$ will increase from zero to the critical value v_m (acceleration period), and it will stay at this value for a certain period of time (constant velocity period), and then decrease to zero right at the ending time t_e (deceleration period). Plan II: if z_e is small, $\dot{z}$ will increase from zero to a certain value, not greater than v_m, (acceleration period), and then decrease to zero right at the ending time t_e (deceleration period). Plan II does not have the constant velocity period. In both plans mentioned above, the vehicle velocity is always non-negative. So, we can rewrite Eq. (5) as follows:

$$A\ddot{z} + C\dot{z}^2 + N = U \tag{8}$$

Setting net force:

$$F = U - N \tag{9}$$

Eq. (8) becomes:

$$A\ddot{z} + C\dot{z}^2 = F \tag{10}$$

Assuming that $U_1 \le U \le U_2$, we have $F_1 \le F \le F_2$ ($U_1, F_1 < 0$ designed reverse forces, U_2, $F_2 < 0$ designed forward forces). EETs can be obtained by solving Eq. (10) either with $F = F_1$ (corresponding to $U = U_2$) for the constant velocity and acceleration periods or with $F = F_1$ ($U = U_1$) for the deceleration period.

1. EFTs with the Constant Velocity and Acceleration Periods

Eq. (10) is rewritten as follows:

$$A\ddot{z}_d + C\dot{z}_d^2 = F_2 \tag{11}$$

The constraints for these periods are: A, C, $F_2 > 0$; and $\dot{z}_d$, $\ddot{z}_d \ge 0$. At the beginning time t_0, the initial conditions are: $\dot{z}_d (t = t_0 = 0) = v_0 = 0$, and $z_d (t = t_0 = 0) = z_0 = 0$. Here, t denotes the variable of time.

Setting

$$\dot{z}_d = u(t) \ge 0 \tag{12}$$

we have:

$$\ddot{z}_d = \frac{du(t)}{dt} \tag{13}$$

Substituting Eqs. (12) and (13) into Eq. (11) yields:

$$A\frac{du}{dt} = F_2 - Cu^2 \tag{14}$$

If $F_2 - Cu^2 \neq 0$, from Eq. (14), we have

$$A\frac{du}{F_2 - Cu^2} = dt \tag{15}$$

or

$$\frac{-A}{C}\frac{du}{u^2 - F_2/C} = dt \tag{16}$$

Finding the antiderivative of each function at both sides of Eq. (16), we obtain:

$$\frac{-A}{2\sqrt{CF_2}}\ln\left|1-\frac{2\sqrt{F_2/C}}{u+\sqrt{F_2/C}}\right|=t+c_1 \tag{17}$$

From Eq. (11), we have $C\dot{z}_d^2 = F_2 - A\ddot{z}_d \le F_2$. So, $u = \dot{z}_d \le \sqrt{F_2/C}$. Therefore, Eq. (17) can be deduced as follows:

$$\frac{-A}{2\sqrt{CF_2}}\ln\left(\frac{2\sqrt{F_2/C}}{u+\sqrt{F_2/C}}-1\right)=t+c_1 \tag{18}$$

Solving for u in Eq. (18), we have the expression of velocity as follows:

$$\dot{z}_d = u = \frac{2\sqrt{F_2/C}}{1+\exp\left[-2(\sqrt{C.F_2}/A)(t+c_1)\right]}-\sqrt{F_2/C} \tag{19}$$

From Eq. (19), we can easily deduce:

$$\begin{cases}\ddot{z}_d = \dfrac{d\dot{z}_d}{dt} = \dfrac{4F_2}{A}\dfrac{\exp\left[-2(\sqrt{CF_2}/A)(t+c_1)\right]}{\left(1+\exp\left[-2(\sqrt{CF_2}/A)(t+c_1)\right]\right)^2}\\ z_d = (A/C)\ln\left(1+\exp\left[2(\sqrt{CF_2}/A)(t+c_1)\right]\right)-\sqrt{F_2/C}t+c_2\\ c_1 = \dfrac{-A}{2\sqrt{CF_2}}\ln\left(\dfrac{2\sqrt{F_2/C}}{v_0+\sqrt{F_2/C}}-1\right)-t_0\\ c_2 = z_0-(A/C)\ln\left(1+\exp\left[2(\sqrt{CF_2}/A)(t+c_1)\right]\right)+\sqrt{F_2/C}t_0\end{cases} \tag{20}$$

If $F_2 - Cu^2 = 0$, we have:

$$u^2 = F_2/C \tag{21}$$

or

$$\dot{z}_d(t) = u = \sqrt{F_2/C} = \text{constant} \tag{22}$$

$\dot{z}_d = \sqrt{F_2/C}$ in Eq. (22) is accepted if the initial time is denoted by t_1 instead of t_0, $t_1 \neq t_0$, and the following initial conditions are satisfied: $\dot{z}_d(t_1) = v_1 = \sqrt{F_2/C} = v_m$ (critical velocity), and $z_d(t_1) = z_1$. In fact, this is a particular case in which the velocity has reached the critical value. At this time, the net force is balanced with the drag force $C\dot{z}_d^2$, the vehicle velocity no longer changes and stays at the critical velocity $\sqrt{F_2/C}$. So, the vehicle acceleration is zero and the vehicle depth increases linearly with time.

$$\begin{cases}\ddot{z}_d(t) = 0\\ \dot{z}_d(t) = u = \sqrt{F_2/C}\\ z_d(t) = \sqrt{F_2/C}t + c_3\\ c_3 = z_1 - \sqrt{F_2/C}t_1\end{cases} \tag{23}$$

2. EETs with the Deceleration Period

Eq. (10) is similarly rewritten as follows:

$$A\ddot{z}_d + C\dot{z}_d^2 = F_1 \tag{24}$$

The constraints for this period are: A, $C > 0$; $F_1 < 0$; $\dot{z}_d \ge 0$; and $\dot{z}_d \le 0$. Assuming that t_2 is the initial time of this period, the corresponding initial conditions are: $\dot{z}_d(t_2) = v_2 > 0$, and $z_d(t_2) = z_2$. Solving Eq. (24), we have the expressions of z_d, $\dot{z}_d$ and $\ddot{z}_d$ as follows:

$$\begin{cases}z_d(t) = (A/C)\ln\left|\cos\left[-(\sqrt{-CF_1}/A)(t+c_4)\right]\right|+c_5\\ \dot{z}_d(\mathrm{t}) = \sqrt{-F_1/C}\tan\left[-(\sqrt{-CF_1}/A)(t+c_4)\right]\\ \ddot{z}_d(\mathrm{t}) = (F_1/A)\Big/\cos^2\left[-(\sqrt{-CF_1}/A)(t+c_4)\right]\\ c_4 = -\left(A\Big/\sqrt{-CF_1}\right)\arctan\left(v_2\Big/\sqrt{-F_1/C}\right)-t_2\\ c_5 = z_2-(A/C)\ln\left|\cos\left[-(\sqrt{-CF_1}/A)(t_2+c_4)\right]\right|\end{cases} \tag{25}$$

The profiles of the EETs for Plan I and Plan II are described in Loc et al. (2014). The ending depth z_e of vehicles in Plan I has large value (long travel distance) and satisfies the inequality: $z_e > z_e^* = z_1^* + \Delta z_3^*$. Otherwise, the ending depth z_e of vehicles in Plan II has small value (short travel distance) and satisfies the inequality: $z_e \le z_e^*$. Where, z_1^* is the distance travelled during the period from the initial time t_0 to the time t_1^* when the vehicle velocity just reaches the maximum value v_1^* (or v_m), and Δz_3^* is the distance travelled during the period from the time when the vehicle velocity starts decreasing from the maximum value v_m to the ending time t_e when it just falls to zero.

If $z_e > z_e^*$ (long range), Plan I trajectories can be divided into four segments in a sequence and the optimal times, velocities, and depths of each segment are expressed as follows:

$$\begin{cases}t_1 = \dfrac{-A}{2\sqrt{CF_2}}\ln\left(\dfrac{1-\xi}{1+\xi}\right)-c_1\\ t_2 = t_1^* + \dfrac{(z_e - z_e^*)}{v_m}\\ t_3 = t_e = -c_4\end{cases} \tag{26}$$

$$\begin{cases} v_1 = \xi\sqrt{\dfrac{F_2}{C}} \simeq v_m \\ v_2 = v_m \\ v_3 = v_e = 0 \end{cases} \tag{27}$$

$$\begin{cases} z_1 = z_1^* = z_{d1}(t_1^*) \\ z_2 = z_e - \Delta z_3^* \\ z_3 = z_e\,(given) \end{cases} \tag{28}$$

The value of ξ is verified by experiments by selecting the optimal value so that the time when the velocity, in the mathematical model, reaches ξ. v_m is equal to the time when the velocity, in reality, reaches v_m. That time is t_1^*.

In the short range case, Plan II trajectories are used and they can be divided into three segments in a sequence. Similar to the Plan I trajectories, the expressions of the optimal times, velocities, and depths of each segment are calculated as:

$$\begin{cases} t_1 = t_2 = \dfrac{A}{2\sqrt{CF_2}}\ln X - c_1 \\ t_3 = t_e = \dfrac{A}{\sqrt{-CF_1}}\arctan\left(\dfrac{v_1}{\sqrt{-F_1/C}}\right) + t_1 \end{cases} \tag{29}$$

$$\begin{cases} v_1 = v_2 = \sqrt{F_2/C}\,\dfrac{-1+e^{\frac{2\sqrt{CF_2}}{A}(t_1+c_1)}}{1+e^{\frac{2\sqrt{CF_2}}{A}(t_1+c_1)}} \\ v_3 = v_e = 0 \end{cases} \tag{30}$$

$$\begin{cases} z_1 = z_{d1}(t_1) \\ z_3 = z_e\,(given) \end{cases} \tag{31}$$

In order to solve the above equations, the expressions of the values such as: Δz_3^*, X, n, γ, and l can be calculated sequentially as:

$$\Delta z_3^* = z_e - z_2 = -(A/C)\ln\left(1/\sqrt{1+v_m^2/(-F_1/C)}\right) \tag{32}$$

$$X = n + \sqrt{n^2 - 1} \tag{33}$$

$$n = \frac{\gamma + 0.5l - 1}{\gamma + 1} \tag{34}$$

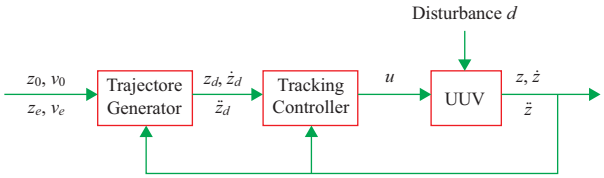

Fig. 2. Depth motion control system block diagram of UV.

$$\gamma = \frac{F_2}{-F_1} \tag{35}$$

$$l = e^{\frac{2C}{A}(z_e - c_2 - \sqrt{F_2/C}c_1)} \tag{36}$$

Moreover, to find t_1, we must solve $\dot{z}_{d1}(t_1) = v_1$. However, mathematically, $\dot{z}_{d1}(t)$ converges exponentially to the maximum value v_m as t tends to infinity. So, we cannot set $v_1 = v_m$ to find t_1. Instead, we will set v_1 nearly equal to v_m as $v_1 = \xi\sqrt{F_2/C} \simeq v_m$, with $\xi < 1$ and $\xi \approx 1$.

IV. TRACKING CONTROLLER

1. Control Algorithm

In this section, we present designing a tracking controller using sliding mode method. The depth trajectory tracking control can be described by the control system block diagram shown in Fig. 2. The model of thruster(s) (actuator) is ignored. The block "*UUV*" contains the depth motion model of the vehicle. The inputs of the block "Trajectory Generator" are the beginning and ending velocities and depths. This block calculates the optimal trajectories and sends them to the block "Tracking Controller". This block contains our controller which determines the control force U required to drive the vehicle for tracking the desired trajectories. Under this control strategy, the UUV will be driven to the desired depth effectively.

The depth motion model of the UV with uncertainties is as follows:

$$A\ddot{z} + C\dot{z}\,|\,\dot{z}\,| + N = U + D \tag{37}$$

In Eq. (37), A, C, N are parametric uncertainties, estimated as $\hat{A}$, $\hat{C}$, $\hat{N}$, respectively. Assuming that $A_{\min} \le A \le A_{\max}$, we have $\hat{A} = (A_{\max} + A_{\min})/2$, and $\Delta A = (A_{\max} - A_{\min})/2$, Likewise for $\hat{C}$, ΔC, $\hat{N}$, and ΔN. D is disturbance, estimated as $\hat{D}$. Assuming that $-d \le D \le d$, we have $\hat{D} = 0$, and $\Delta D = d \ge 0$.

2. Sliding Mode Control Law

The sliding mode method is based on the idea of keeping the scalar quantity s, which is a weighted sum of the position

error $(z - z_d)$, the velocity error $(\dot{z} - \dot{z}_d)$, and (not required) the acceleration error $(\ddot{z} - \ddot{z}_d)$, at zero (Slotine and Li, 1991). Here, the expression of s is chosen as in Eq. (38):

$$s = (\dot{z} - \dot{z}_d) + \lambda(z - z_d) \tag{38}$$

where $\lambda > 0$ is the weight parameter and it must be chosen to be "small" with respect to high-frequency un-modeled dynamics (such as un-modeled structural modes or neglected time-delays). The value of λ is selected based on the frequency range of un-modeled dynamics.

Therefore, the task of the controller is to take s to zero. When s approaches zero, position error (and velocity error, also) approaches zero too, and thus, trajectory tracking is performed. Once s is zero, to keep it at this value, the derivative of s is expected to be zero. From Eq. (38), the expression of $\dot{s}$ can be easily deduced as follows:

$$\dot{s} = (\ddot{z} - \ddot{z}_d) + \lambda(\dot{z} - \dot{z}_d) \tag{39}$$

Substituting the expression of $\ddot{z}$ deduced from Eq. (37) into Eq. (39):

$$\dot{s} = \frac{1}{A}(-C\dot{z}\,|\,\dot{z}\,| - N + U + D) - \ddot{z}_d + \lambda(\dot{z} - \dot{z}_d) \tag{40}$$

To achieve $\dot{s} = 0$, we choose control law as:

$$U = C\dot{z}\,|\,\dot{z}\,| + N + A\ddot{z}_d - \lambda A(\dot{z} - \dot{z}_d) - D \tag{41}$$

Because the parameters C, N, A, and D are unknown and replaced by their estimation $\hat{C}$, $\hat{N}$, $\hat{A}$ and $\hat{D}$, respectively, the control is chosen as:

$$\hat{U} = \hat{C}\dot{z}\,|\,\dot{z}\,| + \hat{N} + \hat{A}\ddot{z}_d - \lambda\hat{A}(\dot{z} - \dot{z}_d) \tag{42}$$

$\hat{U}$ can be seen as our best estimate of the equivalent control. In order to stratify the sliding condition, despite the uncertainty on the dynamics, we add to $\hat{U}$ a term discontinuous across the surface $s = 0$. And, the actual control law which can be robust to uncertainties is the function chosen as follows:

$$U = \hat{U} - K\,\mathrm{sgn}(s) \tag{43}$$

Substituting Eq.(42) into Eq. (43) yields:

$$U = \hat{C}\dot{z}\,|\,\dot{z}\,| + \hat{N} + \hat{A}\ddot{z}_d - \lambda\hat{A}(\dot{z} - \dot{z}_d) - K\,\mathrm{sgn}(s) \tag{44}$$

where, *sgn(.)* is the *signnum* function, defined as:

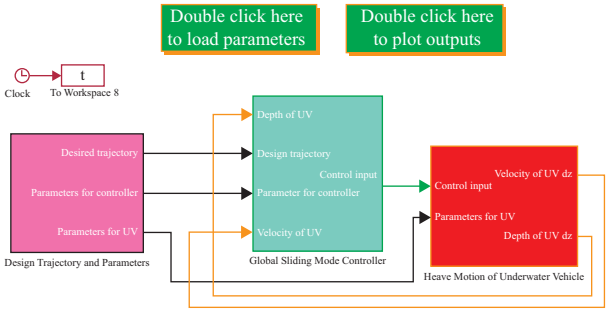

Fig. 3. Simulation program for designing EETs of UV.

$$\mathrm{sgn}(s) = \begin{cases} 1 & \text{if } s > 0 \\ 0 & \text{if } s = 0 \\ -1 & \text{if } s < 0 \end{cases} \tag{45}$$

K is the design parameter chosen to satisfy the sliding condition $\dot{s}s \le -\eta|s| < 0$, with η is a strictly positive constant. Here, we found:

$$\mathrm{K} \ge \Delta C\dot{z}^2 + \Delta A\left|\ddot{z}_d - \lambda(\dot{z} - \dot{z}_d)\right| + \Delta N + d + \eta A_{\max} \tag{46}$$

Generally, the sliding mode controller applied to our system is designed as given in Eq. (44) with K chosen by Eq. (46). To avoid chattering situation by the use of the *sgn(.)* function, we can replace the *sgn(.)* function with the *saturating* function as follows:

$$\mathrm{sat}(s/\phi) = \begin{cases} \mathrm{sgn}(s/\phi) & \text{if } |s/\phi| > 1 \\ s/\phi & \text{otherwise} \end{cases} \tag{47}$$

where, $\phi > 0$ is the boundary layer thickness.

V. SIMULATION AND DISCUSSION

In this section, we analyze the tracking control performance of the UV by using the global optimal sliding mode control, and implement a simulator using a model of the UV. For the simulation, we use a Matlab-Simulink model. The model uses the Matlab-Simulink including three subsystems for the design trajectory and parameters, the global sliding mode controller, and the depth motion dynamic of the vehicle as shown in Fig. 3.

1. System Description

The following simulation is given in order to illustrate the application of the concepts and equations. In this section, we analyze the depth motion behavior of an UV under the influence of the uncertainties, and implement a simulator using the Matlab-Simulink. In the present study, we adopt a commercial UV as the numerical model for calculations. The UV has a length of

Table 1. The estimated values and bounds of the uncertainties.

$\hat{A}$ (kg)	$\hat{C}$ (kg/m)	$\hat{N}$ (N)	$\hat{D}$ (N)	ΔA (kg)	ΔC (kg/m)	ΔN (N)	d (N)
89	52	6	0	17.8	10.4	0	5

Table 2. Controller parameters and designed thrust forces.

λ (s^{-1})	ϕ ($m.s^{-1}$)	η ($m.s^{-2}$)	ξ	U_1 (N)	U_2 (N)
5	0.1	0.001	0.996	0	46

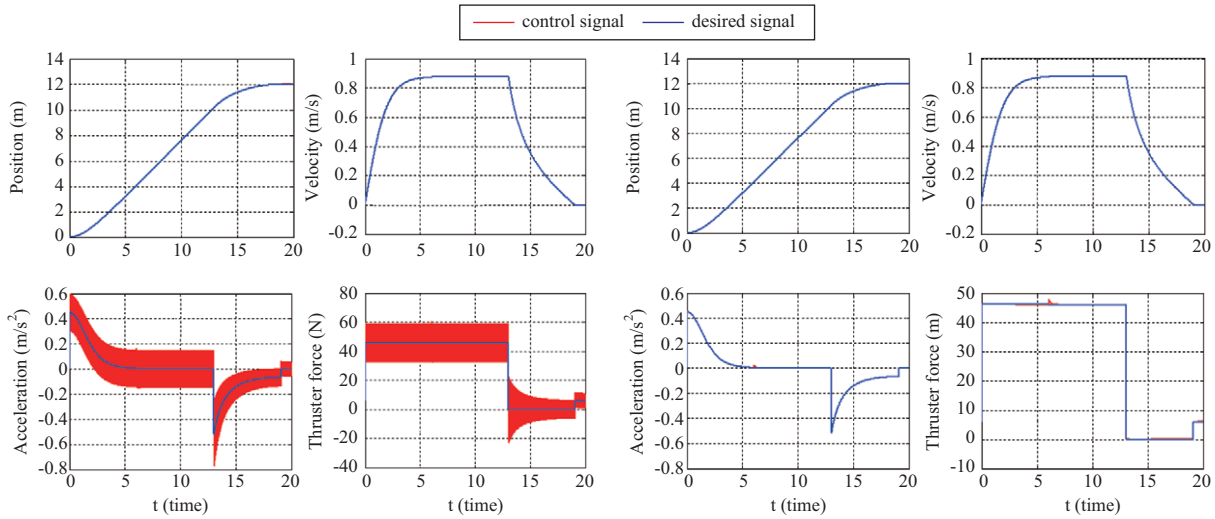

(a) Switched control law (using sign function)

(b) Smooth control law with a thin boundary layer (using saturation function)

Fig. 4. EETs design of Plan I without uncertainties.

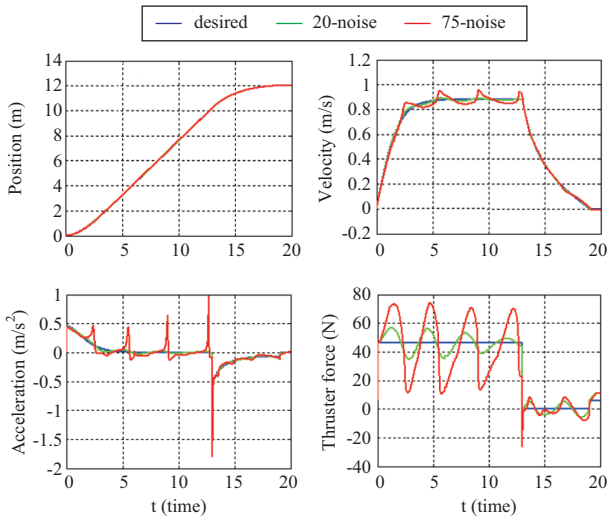

Fig. 5. EETs design of Plan I with uncertainties.

1.5 m and a maximum diameter of 0.18 m as shown in Fig. 1. It is composed of a pressure hull, propulsion system, rudder, elevator, sensors, power supply, communication and navigation systems, etc. The vehicle has buoyancy of 23.8 kgf that is slightly greater than its weight, 23.4 kgf, which allows it to float to the surface in the event of a failure. Its center of buoyancy lies on the vehicle centerline and is higher than its center of gravity; this location promotes stabilization. To further enhance the stability of the vehicle, three fixed planes are installed 120° apart on the aft. To simulate the depth control of the UV using the proposed depth control strategy, all the hydrodynamic coefficients related to the maneuvering characteristics and the variables of the UV set in Vu et al. (2017) were adapted to the model of the UV.

The estimated parameters of the UV model which refer to Chen et al. (2007) and parameters for simulation are shown in Table 1. The parameters a and b are assumed to have 20% uncertainty. The net buoyancy is fixed (no uncertainty). The disturbance d is assumed to be not greater than 5 N in absolute value. In this study, thruster(s) are assumed to have an instantaneous response to the controller's commands of force. The designed thrust forces and the parameters of the controller are listed in Table 2.

2. Simulation for Plan I

The simulation results of the Plan I that explained in Section "EETs with the deceleration period" and Eqs. (26)-(28) are also shown in Figs. 4 and 5. Fig. 4 shows the EETs design without uncertainties in both cases: using sign function and saturation

function, and Fig. 5 shows the EETs design with uncertainties. From these figures, we can observe that proposed SMC has good performance even with the uncertainties. From Fig. 4(a), a chattering effect appears in the control and acceleration signals, which might excite unstable system dynamics, de-gradating the overall controller performance in real-time implementations. The chattering problem in sliding mode control is one of the most common handicaps for applying to real applications. Thus, chattering must be eliminated for the controller to perform properly. In order to overcome the chattering phenomenon, we choose the control signal in Eq. (44) and the results as shown in Fig. 4(b). In this control signal, the sign function is replaced with the saturation function.

In Fig. 4(b), the ending depth is 12 m, which is greater than Δz_e^* = 5.88 m (Plan I). The UV model has no uncertainties. For this case, the ending time is 19.1 s. Segment I lasts from 0 s to 6.062 s, segment II from 6.062 s to 13.04 s, segment III from 13.04 s to 19.1 s, and segment IV from 19.1 s onwards. The control force is almost equal to the designed force (46 N for the constant velocity and acceleration periods, 0 N for the deceleration period) except for the short periods of time at the beginning of each segment. Force deviation in these periods does not exceed 4 N because these are transitional periods of the control system. At rest status (segment IV), the controller maintains a force of 6 N to balance the net buoyancy. This helps the vehicle keep its depth constant. From the simulation results, we can also observe that the acceleration, velocity, and depth of the vehicle track the designed trajectories very well. Maximum absolute errors of the acceleration, velocity, depth are 24.3 mm/s^2, 3.5 mm/s, and 0.58 mm, respectively. The acceleration is about 0.517 m/s^2 at the beginning. It decreases to zero during segment I, and remains at zero in segment II. At the initial point of segment III, it decreases to the peak negative value of -0.517 m/s^2. And then, it increases to -0.067 m/s^2 during segment III. At the initial point of segment IV, it decreases to zero, and stays at this value afterwards. In the case of the velocity, it increases from 0 to 0.877 m/s during segment I, and stays at this value in segment II. And then, it decreases from 0.877 m/s to zero in segment III, and stays at this value of zero afterwards. The controller helps the vehicle move smoothly to the ending depth as shown in Fig. 4. Although the travel time is longer but the energy consumption is minimal.

The simulation results for the EETs design with uncertainties are shown in Fig. 5. In this simulation, EETs of Plan I is used, the ending depth is 12 m. But the controller is applied to the UV model with uncertainties as shown below:

$$A = \hat{A} + \Delta A \sin(2|\dot{z}|t) \tag{48}$$

$$C = \hat{C} + \Delta C \sin(2|\dot{z}|t) \tag{49}$$

$$N = \hat{N} \tag{50}$$

$$D = d \sin(2t + \pi) \tag{51}$$

Our controller is designed based on the assumption that the parameters A and C have 20% uncertainty and the thrust range of the thruster(s) is [-100 100] (N). If the uncertainty of these parameters is greater than 20% such as 75% uncertainty the performance of the controller is still good as shown in Fig. 5.

The existence of the uncertainties forces the controller to give out the commands of force whose values could be greater or less than the designed force. Because the uncertainties are sinusoidal, the control force is also sinusoidal to mitigate their effects as shown in Fig. 5. So, the acceleration and velocity oscillate around the designed trajectories. As shown in Fig. 5, the maximum and minimum control forces in both uncertainty cases are 60.52 N, -22.87 N (20% uncertainties) and 74.55 N, -26.2 N (75% uncertainties), respectively. Similarly, the maximum absolute errors of acceleration, velocity, depth in both cases are 1287 mm/s^2, 89.1 mm/s, and 38.6 mm, respectively. The depth error at steady state (segment IV) does not exceed 3.4 mm. This error could be smaller if the parameter λ was a higher value.

3. Simulation for Plan II

The simulation results of the Plan II that explained in Section "EETs with the deceleration period" and Eqs. (29)-(31) are also shown in Figs. 6 and 7. While Fig. 6 shows the performance with switching control law and smooth control law, Fig. 7 shows the EETs design with uncertainties. We can see there is seriously high frequency chattering in the control and acceleration signals in Fig. 6(a) due to the discontinuous control signal of sign function in control input. Since the sign function is replaced by the saturation function in the control signal, it is shown that the chattering phenomenon has been reduced effectively in Fig. 6(b).

In this simulation, the ending depth is just 2 m, which is less than Δz_e^* = 5.88 m (Plan II). The UUV model has no uncertainties. For this case, the ending time is 7.35 s. Segment I lasts from 0 s to 1.86 s, segment II from 1.86 s to 7.35 s, and segment III from 7.35 s onwards. The results show that the vehicle acceleration is 0.517 m/s^2 at the beginning, and that it decreases to 0.2 m/s^2 during segment I. At the initial point of segment II, it decreases to the peak negative value of -0.32m/s^2. And then, it increases to -0.067 m/s^2 during segment II. At the initial point of segment III, it decreases to zero, and stays at this value afterwards. The results also reveal that the velocity increases from 0 m/s to 0.65 m/s during segment I, and then, decreases to zero in segment II, and maintains this value of zero in segment III. In addition, the control force and the depth track the designed trajectories very well as shown in Fig. 6.

The simulation results for the EETs design of Plan II with uncertainties are shown in Fig. 7. In this simulation, the ending depth is 2 m. In this case, simulation parameters such as initial conditions, system parameters, uncertainty term and controller parameters are selected same as the previous case. Parameter ϕ in the saturation function is selected as ϕ = 0.1 (see Table 2). Our controller is designed based on the assumption that the pa-

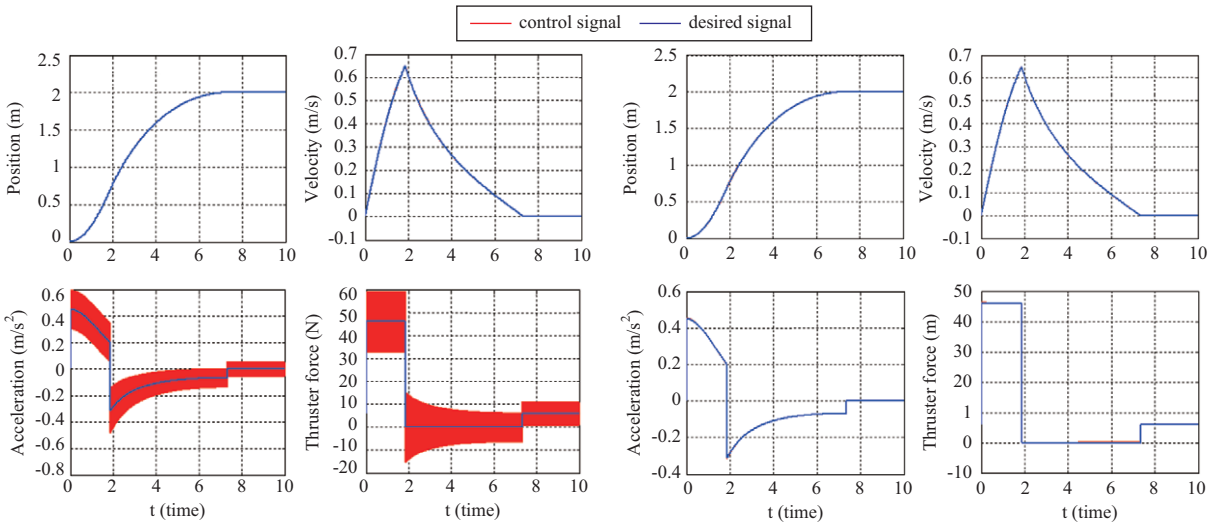

(a) Switched control law (using sign function)

(b) Smooth control law with a thin boundary layer (using saturation function)

Fig. 6. EETs design of Plan II without uncertainties.

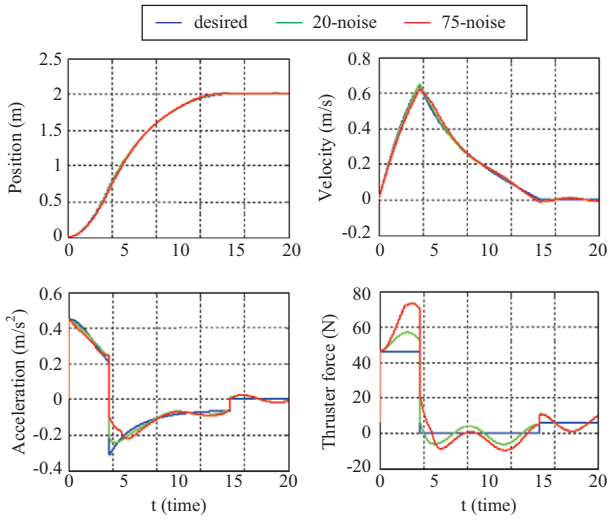

Fig. 7. EETs design of Plan II with uncertainties.

rameters A and C have 20% uncertainty and the thrust range of the thruster(s) is [-100 100] (N). From Fig. 7, we can observe that proposed SMC still has good performance even with 75% uncertainties. Through simulation results, we see that the depth in case of 75% uncertainty can still track the designed depth although the depth error increases to 3.64 cm, and the control force is required to 73.15 N or -9.68 N. Generally, computer simulations show that the novel proposed sliding mode controller not only is effective and feasible to stabilize the chaotic system, but also chattering phenomenon is reduced effectively.

VI. CONCLUSION

In this paper, we propose new EETs design, together with a robust tracking controller. We propose a novel GSMC for an uncertain linear time-varying second order system. The proposed controller was implemented on depth motion control of the UV with uncertainty of bounded parameters and disturbances within limited control input. A good point of the proposed controller is that, as a result of the control action, the arrival time at the reference position and the maximum allowable acceleration are expressed in a closed-form equation if ranges of parametric uncertainties and reference inputs are specified. Furthermore, the capacity of vehicle systems with the condition of the minimum arrival time and energy to the target position can be designed by using this closed-form equation.

To support the validity of the proposed EETs, new GSMC controller, we performed the computer simulation. The effectiveness of the combination of the EETs and the proposed trajectory tracking controller was demonstrated via simulation results. The simulation results show that if there are not the influences of the uncertainties, the control forces of the controller will be nearly equal to the designed constant forces, on the contrary, they could be different. Therefore, the thruster(s) should be chosen so that it can meet the requirements of control force of the controller. In addition, the robustness of the approach can be guaranteed even with uncertainties if bounds of the uncertainties are known.

ACKNOWLEDGMENTS

This research is a part of the project National Research Foundation of Korea (NRF-2016R1A2B4011875) and a part of project titled “R & D center for underwater construction robotics”, South Korea (PJT200539), funded by the Ministry of Oceans and Fisheries (MOF).

REFERENCES

Chyba, M., T. Haberkorn, R. N. Smith and S. K. Choi (2008a). Autonomous

underwater vehicles: Development and implementation of time and energy efficient trajectories. Ship Technology Research 55(2), 36-48.

Chyba, M., T. Haberkorn, R. N. Smith and S. K. Choi (2008b). Design and implementation of time efficient trajectories for an underwater vehicle. IEEE Journal of Ocean Engineering 35(1), 63-76.

Cristi, R., A. F. Papoulias and A. Healey (1990). Adaptive sliding mode control of autonomous underwater vehicle in the dive plane. IEEE Journal of Oceanic Engineering 15(3), 152-160.

Deam, W. and D. Given (1983). ROV technology trends and forecast. OCEANS 15, 573-578.

Fiorelli, E., N. E. Leonard, P. Bhatta, D. Paley, R. Bachmayer and D. M. Fratantoni (2004). Multi-AUV control and adaptive sampling in Moterey Bay. Workshop on Multiple AUV Operations (AUV04), 134-147.

Fossen, T. I. (1994). Guidance and Control of Ocean Vehicles. John Wiley and Sons, New York.

Healey, J. and D. Lienard (1993). Multivariable sliding mode control for autonomous diving and steering of unmanned underwater vehicles. IEEE Journal of Oceanic Engineering 18, 327-339.

Josserand, T. M. (2006). Optimally-robust nonlinear control of a class of robotic underwater vehicles. Doctoral Dissertation, the University of Texas at Austin, USA.

Li, J. H. and P. M. Lee (2005). Design of an adaptive nonlinear controller for depth control of an autonomous underwater vehicle. Ocean Engineering 32(17-18), 2165-2181.

Loc, M. B., H.S. Choi, S.S. You and T.N. Huy (2014). Time optimal trajectory design for unmanned underwater vehicle. Ocean Engineering 89, 69-81.

Moreira, L. and C. Guedes Soares (2008). H_2 and H_∞ designs for diving and course control of an autonomous underwater vehicle in presence of waves. IEEE Journal of Oceanic Engineering 33(2), 69-88.

Prestero, T. (2001). Verification of a six-degree of freedom simulation model for the REMUS autonomous underwater vehicle. Master Thesis, Massachusetts Institute of Technology.

Rodrigues, L., P. Tavares and M. Prado (1996). Sliding mode control of an AUV in the diving and steering planes. MTS/IEEE Oceans, Florida, USA.

Salgado-Jimenez, T., J.-M. Spiewak, P. Fraisse and B. Jouvence (2004). A robust control algorithm for AUV: based on a high order sliding mode. Proceeding of MTTS/IEEE Techno-Oceans'04, Kobe, Japan 1, 276-281.

Slotine, J. J. and W. Li (1991). Applied Nonlinear Control. Prentice Hall.

Stewart, L. L. and P. J. Auster (1989). Low cost ROV's for science. In: Proceedings of OCEANS '89, Seattle, Washington DC, USA.

Stokey, R., B. Allen, T. Austin, R. Goldsborough, N. Forrester, M. Purcell and C. V. Alt (2001). Enabling technologies for REMUS docking: an integral component of an autonomous ocean-sampling network. IEEE Journal of Oceanic Engineering 26(4), 487-497.

Vu, M. T., H. S. Choi, J. I. Kang, D. H. Ji and S. K. Jeong (2017). A study on hovering motion of the underwater vehicle with umbilical cable. Ocean Engineering 135, 137-157.